Correlations between microscopic properties and the photorefractive response for vanadium-doped CdTe

L. A. de Montmorillon, Ph. Delaye, and G. Roosen

Institut d'Optique, Unité de Recherche Associée 14 au Centre National de la Recherche Scientifique, Bât. 503, Centre Scientifique d'Orsay, B.P. 147, 91403 Orsay Cedex, France

H. Bou Rjeily, F. Ramaz, and B. Briat

Laboratoire d'Optique Physique, Unités propres de Recherche A0005 du Centre National de la Recherche Scientifique, École Supérieure de Physique et Chimie Industrielle, 10 rue Vauquelin, 75231 Paris Cedex 05, France

J. G. Gies, J. P. Zielinger, and M. Tapiero

Institut de Physique et Chimie des Materiaux de Strasbourg, Unité mixte 380046, Centre National de la Recherche Scientifique, Université Louis Pasteur, Ecole Européenne des Hautes Etudes des Industries Chimiques de Strasbourg, Groupe d'Optique Nonlinéaire et d'Optoélectronique, 23 rue du Loess, F-67037 Strasbourg Cedex, France

H. J. von Bardeleben

Groupe de Physique des Solides, Unité de Recherche Associée 17 au Centre National de la Recherche Scientifique, Université Paris 6 et 7, 2 Place Jussieu, 75231 Paris Cedex 05, France

T. Arnoux and J. C. Launay

Action Aquitaine de Recherche en Apesanteur, B.P. 11, 33165 Saint Médard en Jalles Cedex, France, and Institut de Chimie de la Matière Condensée de Bordeaux, Av. du docteur A. Schweitzer, 33608 Pessac Cedex, France

Received February 12, 1996; revised manuscript received April 26, 1996

We present a summary of the experimental results, the attempts of interpretation at the present stage, and the conclusions of coupled investigations on semi-insulating, n-type and p-type vanadium-doped CdTe crystals. Combining electron paramagnetic resonance and magnetic circular dichroism permits the monitoring and the quantitative assessment of $[V^{2+}]$ and $[V^{3+}]$ defect concentrations. Photoabsorption results are presented and are discussed in terms of photoionization processes at various wavelengths. The temperature and the spectral dependence of the steady-state photoconductivity are carefully studied in the near infrared. The results are discussed in terms of electronic transitions for the two vanadium charge states. Finally, the photorefractive performances of the semi-insulating sample are analyzed in a two-beam-coupling experiment and are correlated to the properties of the V^{2+}/V^{3+} donor states to derive photoionization cross sections. © 1996 Optical Society of America.

1. INTRODUCTION

We have shown in a recent paper[1] that the combination of different measurements permits a good simulation of the photorefractive properties of GaAs crystals. We used electron paramagnetic resonance (EPR) measurements to determine the $EL2^{+}$ concentration and absorption measurements to determine the total EL2 concentration and took the photoionization cross sections in the literature to calculate the expected photorefractive gain of our sample at different wavelengths and to compare it with the experimental data. The results were found to be consistent, confirming that the EL2 defect was the deep defect responsible for the photorefractive effect in GaAs and that the photorefractive model of one defect coupled to both conduction and valence bands explained well the photorefractive performances in this material.

In this paper we use a similar approach for another photorefractive material, vanadium-doped cadmium telluride (CdTe:V). This photorefractive material is presently the object of great interest as a promising candidate for a use in metrology systems and optical telecommunication networks in the wavelength range from 1 to 1.55 μm. Beyond the control of imperfections and residual impurities, one of the problems is to learn which factors control the concentrations of V^{2+} and V^{3+} ions in CdTe:V. To this end it is important to be able to determine the thermal and the optical signatures of both ions and their respective roles as absorption, trapping, or recombination centers, as well as their respective concentrations. To

0740-3224/96/1002341-11$10.00

Table 1. Electrical Characteristics of the Different Samples Studied in the PC Experiments[a]

Sample	Type	Nature	Dark Resistivity (Ω cm) at Room Temperature	Activation Energy (eV)
L825	Intrinsic	Undoped CdTe Starting material	10^8	0.76
B23	*n*	CdTe:V	1×10^{10}	0.75
B28	*p*	As-codoped CdTe:V	3×10^9	0.74
B19	*n*	Cl-codoped CdTe:V	6×10^8	0.51

[a] L825 is an undoped CdTe crystal used as a reference sample.

see the V^{2+} (V^{3+}) charge state independently, codoping with Cl (As) transforming semi-insulating CdTe:V into *n*- (*p*-) type crystals is used. Table 1 indicates some of the properties of these crystals. We perform in these CdTe:V samples different optical, electrical, and photorefractive (in the semi-insulating one) measurements that give us information about deep defects and their optical properties. Then the determined parameters are combined, allowing us to identify the deep level involved in the photorefractive effect.

Section 2 deals with an EPR study of the different crystals. The EPR results have allowed us to determine the Fermi-level position and the corresponding V configurations in the codoped samples, to measure quantitatively the V^{3+} defect concentrations[2–7] and to test the directly photoinduced variations of the V^{3+} charge state in the semi-insulating (B23) sample. Section 3 deals with a magneto-optical study of the different crystals. This includes magnetic circular dichroism (MCD) and optical absorption spectroscopy. By use of EPR for the quantitative assessment of $[V^{3+}]$ in at least one sample, MCD provides both $[V^{3+}]$ and $[V^{2+}]$. Linked to this, photoabsorption data give information about the photogeneration of carriers from the identified deep levels. Section 4 concerns photoconductivity (PC) studies. We measure the temperature dependence of the steady-state PC gain at the intrinsic maximum (band-to-band excitation), as well as the steady-state spectral response of PC at constant photon flux for varying temperatures of as low as 81 K. Section 5 deals with detailed photorefractive measurements on sample B23. Section 6 is a general discussion concerning the correlations among all our results to provide information about spectroscopic assignments, charge-transfer processes, or photoionization cross sections. The paper ends with a brief summary.

2. ELECTRON PARAMAGNETIC RESONANCE STUDIES

To associate the different optical absorption bands with the particular charge states of the V donor we prepared donor, Cl (B19), and acceptor, As (B28), codoped samples. As the V donor introduces a deep level at $\approx E_c - 0.8$ eV, the EPR observation of the neutral shallow donor Cl^0 with a level at $E_c - 0.02$ eV or the deep ionized donor Fe^{3+} (residual contamination) with a level at $E_v + 0.35$ eV allows us to conclude whether the V donor is completely in the V^{2+} or the V^{3+} charge state. Figure 1 shows the EPR spectra of the B19, the B23, and the B28 samples. In sample B19 only the spectrum of the Cl effective mass donor with a *g* factor $g \approx 1.7$ is observed. In this sample the V donor is in the V^{2+} charge state. Even though this state is equally paramagnetic, the corresponding EPR spectrum is not observed; this has been attributed to the strain sensitivity of the orbital triplet ground state. Sample B19 is used below to identify the V^{2+}-related absorption bands; in contrast, in the acceptor (As) codoped sample (B28), we observe in thermal equilibrium the Fe^{3+} resonance, which allows us to situate the Fermi-level below $E_v + 0.35$ eV and thus below the V donor level. Sample B28 is used below for identification of the V^{3+}-related optical absorption bands.

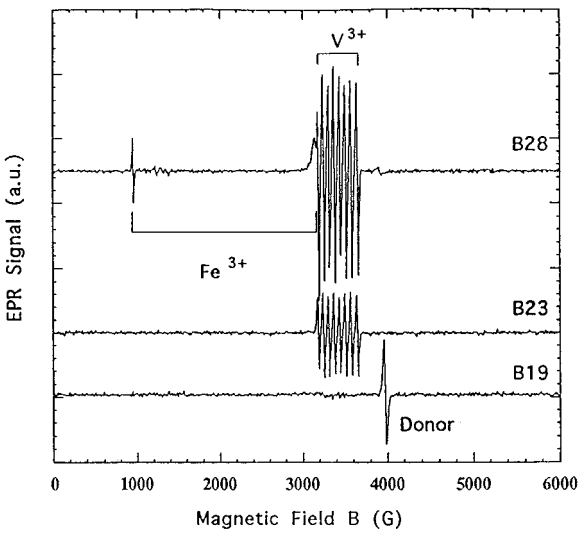

Fig. 1. EPR spectra of the three samples B19, B23, and B28 at $T = 4$ K and $\mathbf{B}\|[100]$. In the *n*-type (B19) codoped sample only the donor resonance is seen, in B23 we observe only the V^{3+} spectrum (no V^{2+}), and in the *p*-type codoped sample B28 both V^{3+} and Fe^{3+} (Fe contamination) is observed.

For the modeling of the photorefractive properties of sample B23 the absolute V^{3+} concentration is required; it has been determined by comparison with a spin-standard sample.

The photoionization of the V donor in sample B23 can also be directly studied by EPR by means of the associated changes in the V^{3+} concentration. We tested the influence of an optical excitation at the two relevant wavelengths of 1.06 and 1.4 μm. As shown in Fig. 2, a 1.06-μm excitation increases the V^{3+} concentration, whereas the 1.4-μm excitation is associated with a decrease of the V^{3+} concentration. From this result we can

qualitatively conclude that the associated photoionization cross sections for electrons (S_n) and holes (S_p) are $S_n > S_p$ at 1.06 μm and $S_n < S_p$ at 1.4 μm.

3. MAGNETO-OPTICAL AND OPTICAL ABSORPTION STUDIES

A. Magnetic Circular Dichroism

MCD is the differential absorption ($\Delta\alpha$ in cm^{-1}) for left (σ_+) and right (σ_-) circularly polarized lights propagating along the direction of an applied magnetic field **B** (typically 2.5 T). The MCD signal contains, in general, a diamagnetic as well as a paramagnetic part, but the former can safely be ignored in our case because the bands are broad, and we conduct our work at $T \leqslant 4.2$ K. In the case of, e.g., V^{3+} (with a $^3A_2$ ground state), the paramagnetic terms are proportional to $(n_- - n_+)/(n_0 + n_- + n_+)$, where n_+, n_-, and n_0 stand for the Boltzmann populations of the $m_s = \pm 1$ and the $m_s = 0$ substates.

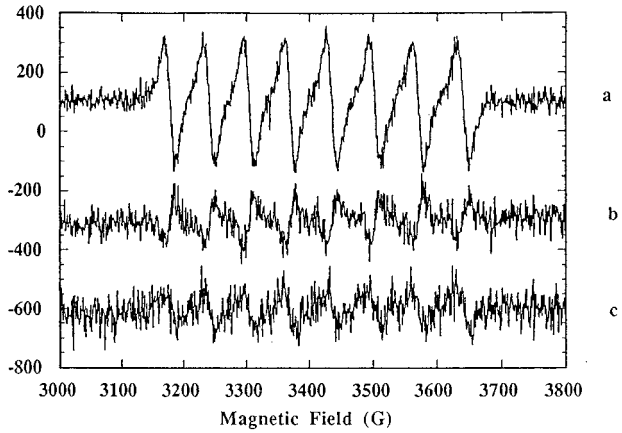

Fig. 2. (a) EPR spectrum of sample B23 at thermal equilibrium at $T = 4$ K. (b), (c) Difference spectra (spectrum under photoexcitation minus spectrum in thermal equilibrium). At 1.4 μm (b), we thus observe a decrease in the V^{3+} intensity; at 1.06 μm (c), an increase, always compared with the thermal equilibrium value. Typical excitation intensities are 10 $\mu W\,cm^{-2}$, and the spectrum intensity achieves an equilibrium value after typically a few minutes.

In a recent paper[8] we demonstrated that this technique permits the simultaneous monitoring at $T \leqslant 4.2$ K of the two paramagnetic species $[V^{2+}]$ and $[V^{3+}]$ in CdTe:V crystals. It was further used in the case of Zn–Cd alloys[9] to show that V^{3+} was present in them, although EPR failed to detect it directly.

Figure 3 shows additional results for our reference crystal B23 (semi-insulating) as well as for n-type (B19) and p-type (B28) samples. Following our former research,[8] the various MCD features are referred to as $P_1, P_2, \ldots, P_5$ (or 1...5 for short). Band P_1 is associated with the major MCD band peaking at ~1.17 eV (9500 cm^{-1}). As expected, samples B19 and B28 indeed present a completely different behavior. Below 1.05 eV [Fig. 3(a)] the former shows only P_2, whereas the latter presents two major bands, P_3 and P_4, and a relatively sharp negative peak, P_5. A Gaussian analysis actually strongly suggests the presence of an additional broad component, P_6, on the high-energy side of P_4. We assigned[8] P_5 to the $^3A_2 \rightarrow {}^1E$ spin-forbidden band of V^{3+} on the basis of its sharpness and negative MCD. It is quite remarkable (Fig. 3) that the MCD spectra of samples B19 (multiplied by 1.4) and B23 superimpose each other in the regions of bands P_1 and P_2. This confirms our earlier findings[8] with two other crystals (B16 and B21), and we assign both bands to V^{2+}.

The low-energy MCD of sample B23 is clearly (Fig. 3) a linear combination of those of the two model compounds. The relative strength of P_4 (and P_3) in B28 and B23 is found to be 6 [Fig. 3(a)], in perfect agreement with EPR (Fig. 1), which gives $[V^{3+}] = 6 \times 10^{15}$ cm^{-3} for B23 and $[V^{3+}] = 35 \times 10^{15}$ cm^{-3} for B28.[4] Concerning the calibration of the MCD P_2 band related to V^{2+}, we have

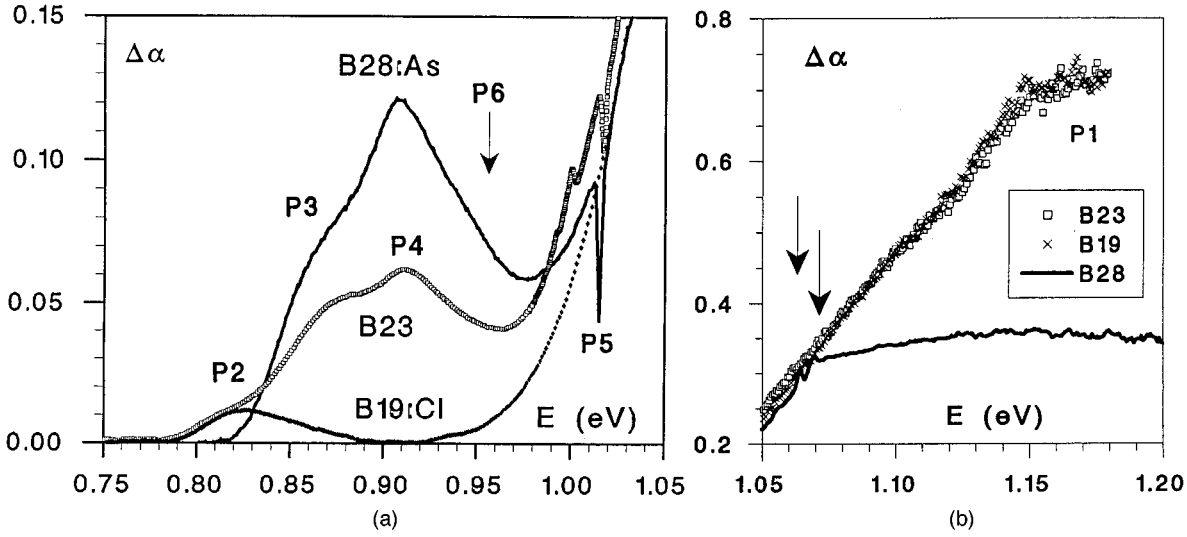

Fig. 3. MCD spectra of samples B28 (codoped As), B19 (codoped C2), and B23 under a magnetic field of 2.5 T at 1.4 K. $\Delta\alpha$ is expressed in inverse centimeters: (a) low-energy region, (b) high-energy region. The ordinate scales apply to sample B23. For comparison, $\Delta\alpha$ for B19 was multiplied by 1.4, whereas $\Delta\alpha$ for B28 was divided by 3 (see text for discussion).

Table 2. Determination of $[V^{3+}]$ and $[V^{2+}]$ in the Five Crystals Investigated[a]

Sample	$[V^{3+}]_{EPR}$	$[V^{3+}]_{MCD}$	$[V^{2+}]_{MCD}$	$R = [V^{2+}]_{MCD}/[V^{3+}]$
B16	7	7	3.5	0.5
B19	0	~0	3.2	
B20		~0	4.9	
B21		14	18	1.3
B23	6	6	4.7	0.8
B28	35	35	0	

[a] The calibration of $[V^{3+}]$ from the MCD follows the EPR measurement on sample B28. That of $[V^{2+}]$ results from a conjugation of MCD measurements on bands P_1 and P_2 as well as photo-MCD data on sample B21. Sample B20 was doped with cadmium chloride. The common unit is 10^{15} at cm^{-3}.

proposed[8] a procedure that rests upon the assumption that the photoconversion process in semi-insulating crystals concerns essentially the V^{2+}/V^{3+} state. We have performed photo-MCD measurements at 1.4 K on a sample (B21) for which bands P_2 and P_4 are of relatively similar strength. We found that a 15-min illumination at 1.06 μm with a Nd:YAG laser (10 mW) increases the strength of bands P_4 and P_3 by 8% ± 0.4%, whereas it decreases that of P_2 by 6% ± 2%. It is then a simple matter to establish[8] that the ratio of the relative change of the MCD for P_4 on the one hand to that for P_2 on the other is equal to $R = [V^{2+}]/[V^{3+}] = 1.3 \pm 0.4$. Because $[V^{3+}] = 14 \times 10^{15}$ cm^{-3} for this sample, one therefore finds that $[V^{2+}] = 18 \times 10^{15}$ cm^{-3}. MCD provides us with the relative strength of band P_2 for samples B21 and B23; we were thus able to estimate $[V^{2+}] \approx 5 \times 10^{15}$ cm^{-3} ($R \approx 0.8$) for sample B23. We also performed a photo-MCD experiment on B23. It showed a 10% increase of P_3–P_4 under an illumination at 1.06 μm. Unfortunately, we could not reliably estimate the relative change of P_2 because the expected absolute change is only twice the noise level and because bands P_2 and P_3 overlap slightly [compare B19 and B28 in Fig. 3(a)]. Table 2 presents our overall concentrations results for six crystals investigated in the course of this study or of our previous study.[8] Our model is predictive, and Fig. 4 shows the MCD spectra expected in the low-energy region for various R ratios. Although the absolute scale obviously depends on $[V^{2+}] + [V^{3+}]$, the shape (at 1.4 K) rests solely on R.

We note that band P_5 for B23 is preceded [Fig. 3(a)] by two weak positive MCD features at 8020 cm^{-1} (0.994 eV) and 8080 cm^{-1} (1.002 eV). Whether they are associated with spin-forbidden lines of V^{2+} or are origin lines for spin-allowed transitions is presently unknown. We have of course verified that the nominally undoped crystal (L825) did not show any of the features $P_1 \ldots P_6$ discussed here.

In the higher-energy region [Fig. 3(b)], one may wonder whether band P_1 is present to a certain extent for sample B28. With normalization of the MCD spectra of B28 and B23 for bands P_3–P_4, it is seen that the MCD of B28 at 1.17 eV is only 25% of the intensity of band P_1. Furthermore, the MCD shape is very different for the two materials, and B28 shows two additional MCD lines [see arrows in Fig. 3(b)]. We confirm therefore that B28 contains either none or a negligible amount of V^{2+}. The MCD features at higher energies are presumably related to arsenic.

B. Absorption and Photoabsorption

Our measurements were performed on a Cary 05E spectrometer. For photoabsorption experiments, the crystal at thermal equilibrium is cooled down to 80 K in a cold finger cryostat and a first spectrum (called init) is taken. The crystal is then illuminated 10 min *in situ* (nothing moves) with the spectrometer at a wavelength λ_1, and a second spectrum "λ_1" is taken immediately after the illumination is switched off. The procedure is repeated for several decreasing illuminating wavelengths $\lambda_2 \ldots$. We interest ourselves in differences (noted "λ_1 − init" or "$\lambda_n - \lambda_{n-1}$") between successive spectra. Finally, the illumination at 1.55 μm is repeated at the end of the experiment.

Figure 5 shows the absorption spectrum at 80 K of sample B23 as well as those for the two model compounds B19 and B28. This figure confirms that these last two spectra do represent two extreme situations that bear no resemblance to each other. Band 5 is too weak to be detected in optical absorption, but bands 2–4 are clearly observed. We note that band 6 (approximately 0.96 eV), which seemed to be necessary to understand the MCD spectrum of sample B28, is now clearly seen in its absorption spectrum. Cooling the crystals from room temperature to liquid-nitrogen or liquid-helium temperature results in a very clear blue shift of at least 40 meV (300 cm^{-1}) and in a noticeable sharpening of the major absorption components, thus revealing an important role of phonon broadening. We note that the absorption spectrum of B23 is qualitatively similar to that reported in Refs. 6, 8, and 10.

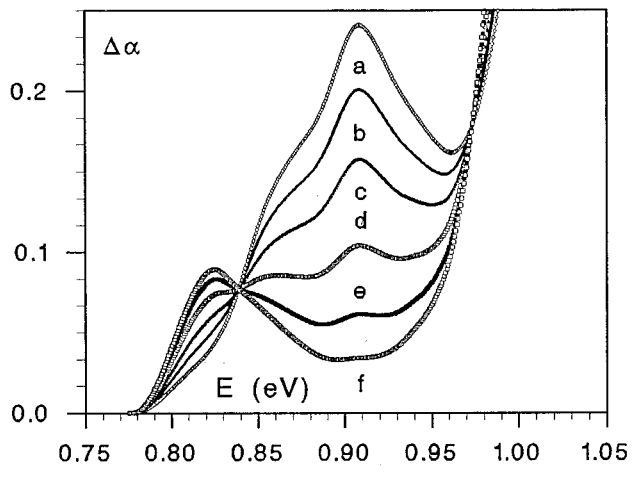

Fig. 4. Predicted MCD spectra at 1.4 K and under 2.5 T according to the ratio R of $[V^{2+}]$ and $[V^{3+}]$. We arbitrarily assumed a total vanadium concentration T of 35 (unit, 10^{15} cm^{-3}). From top to bottom at 0.91 eV, the various curves stand for values of R: (a) 0.5, (b) 0.8, (c) 1.3, (d) 2.5, (e) 5, and (f) 10. We computed these by combining those for B19 ($[V^{2+}] = 3.2$) and B28 ($[V^{3+}] = 35$) with the weighting factors $(T/3.2) * R/[(1 + R)]$ and $(T/35)/(1 + R)$, respectively.

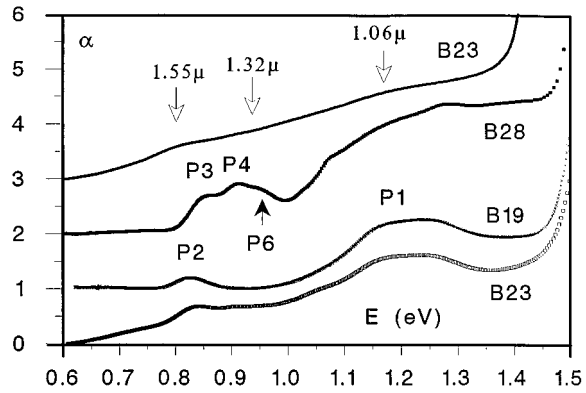

Fig. 5. Absorption spectra of samples B28, B19, and B23 at 80 K (three lower curves) and B23 at room temperature (upper curve). α is expressed in inverse centimeters. For clarity, the residual absorption at 0.6 eV was subtracted from each of the curves; they were then translated by 1 cm^{-1} from one another at the same energy. The numbering of the various features is the same as that shown in Fig. 1. Note that, although taken from the same ingot, the B19 sample used for absorption is of a much better quality (no scattering) than that examined in our earlier study.[8]

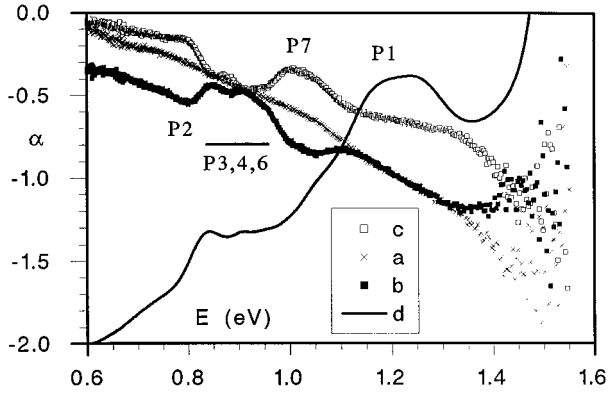

Fig. 6. Photoabsorption results for sample B23 at 80 K. Spectrum a stands for the difference of absorbance (multiplied by 20), "1.32 − init" (see Subsection 3.B for explanation). Spectrum *b* deals with "1.06 − 1.32," whereas spectrum c is associated with "1.55*b* − 1.06." The absorption spectrum (shifted by -2 cm^{-1}) is also given (d) for comparison.

Absorption spectra in the low-energy region could in principle be analyzed in a fashion similar to MCD spectra analysis. This is, however, very difficult because the absorption features eventually superimpose over an energy-dependent background, which is presumably due in part to scattering. Beyond its sensitivity, an additional advantage of MCD over absorption is that $\Delta\alpha/\alpha$ is much stronger for bands P_3–P_4 than for band P_2, with the former thus sometimes being hardly resolved in the absorption spectrum.[6,10–12]

Figure 6 shows photoabsorption data (on sample B23), for the first time to our knowledge. Illumination was of course carried out with those wavelengths used for photorefractive[13] or photo-EPR experiments.[2] The difference spectra "1.55*a* − init" and "1.32 − 1.55" [see Fig. 6(a)] show essentially a monotonic behavior. By contrast, a further illumination at 1.06 μm leads to a significant increase of bands P_3, P_4 (but also P_6) and a decrease of band P_2 [Fig. 6(b)]. Our results also indicate that component P_7 (0.98–1.10 eV), which is seen in our absorption spectrum at 80 K [Fig. 6(d)] as well as in that at 6 K (Ref. 12), behaves like band P_2 in this process and is therefore probably correlated with the presence of V^{2+}. A further illumination at 1.55 μm ["1.55*b* − 1.06" in Fig. 6(c)] reverses the situation. These data are in excellent agreement with the experimentally observed dominance (see Sections 2 and 5) of hole carriers at 1.55 μm and electron carriers at 1.06 μm. Somewhat surprisingly, illumination has no marked effect on band P_1.

4. PHOTOCONDUCTIVITY STUDIES

Concerning the experimental point of view, particular care was devoted to providing the samples with closely spaced (1–2 mm) stable ohmic contacts and to achieve preliminary electrical and photoelectrical characterization. Two kinds of measurements, among those that were performed, are presented here: (i) temperature dependence of steady-state PC gain at the intrinsic maximum (band-to-band excitation) and (ii) steady-state spectral response of the PC at constant photon flux, for varying temperature.

A. Dependence of the Intrinsic Photoconductivity Gain on Temperature

We obtained the temperature dependence of the photocurrent by plotting the saturation value of the PC of the sample under continuous monochromatic illumination. The maximum intrinsic (band-to-band) PC near the absorption edge occurs for the wavelength $\lambda = \lambda_{max}$, corresponding to an absorption constant, $\alpha_{max} \sim 1/d$, where d is the thickness of the specimen.[14] During the temperature scan, λ_{max} was continually adjusted to achieve the maximum photoresponse, so that the optical generation rate of photocarriers $\alpha_{max}\Phi_0 = \Phi_0/d$ (where Φ_0 is the incident photon flux) is temperature independent.

The general equation expressing the PC,[14] from a phenomenological point of view, is

$$i_{ph} = AEq(\mu_n\tau_n + \mu_p\tau_p)\alpha\Phi_0, \tag{1}$$

where i_{ph} is the steady-state photocurrent; q, the electronic charge; A, a constant depending on the geometry of the sample; E, the electric field; α, the absorption coefficient; and Φ_0, the incident photon flux, corrected for reflection losses. Here μ_n, μ_p denote, as usual, the drift mobilities of the free photoelectrons and photoholes, respectively, and τ_n and τ_p denote their lifetimes, respectively.

It is convenient to consider the intrinsic PC in terms of a gain G, which is defined as the number of charge carriers passing between the electrodes for each photon absorbed per second.[15] This can be written in the form

$$i_{ph} = qAEG\alpha\Phi_0 \tag{2}$$

if one wants to express the PC gain independent of the experimental conditions (size of the sample, electric field).

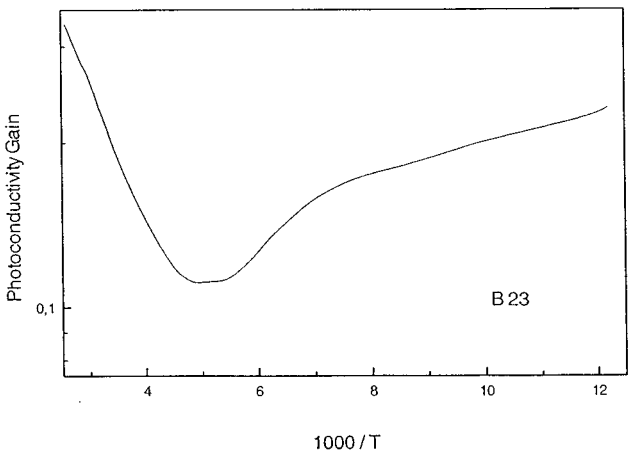

Fig. 7. Thermal dependence of the PC gain for sample B23. The ordinate unit is arbitrary.

The gain G, which can also be considered as a kind of photosensitivity,[15] is a crucial parameter and is found to be equal, at room temperature, to ~0.35 for sample B23. Comparison of Eqs. (1) and (2) shows that

$$G = \mu_n \tau_n + \mu_p \tau_p \tag{3}$$

and depicts a material property in terms of the $\mu\tau$ product.

It appears that the thermal variation of PC gives the temperature dependence of the product $\mu\tau$.

Figure 7, obtained for specimen B23, shows that the gain increases fairly exponentially with $1/T$ (with two activation energies of approximately 20 and 5 meV) for measurements roughly below 180 K, which is close to the Debye temperature [158 K (Ref. 16)]. If one assumes that the variation of the gain in this temperature range is due mainly to the lifetime; with that of the mobility being considered negligible, then these activation energies may correspond to acoustic phonons (~5 meV) and to optical phonons (~20 meV), in agreement with the values found in Ref. 17.

Above 200 K, in contrast, a decrease is observed when $1/T$ increases, with an activation energy of 63 meV. This may be explained by the fact that in this range of temperature the V^{2+}/V^{3+} levels empty, making the recombination centers less active and permitting the increase of the free-electron lifetime.

It is noteworthy that the variation of the PC gain varies moderately with temperature, less than a factor of 4, and modulates, as is shown below, the spectral responses at temperatures higher than 180 K.

B. Spectral Response of Steady-State Photoconductivity at Room Temperature

The steady-state PC spectra were measured at ~300 K for samples B23 (CdTe:V), B28 (CdTe:V, As), and B19 (CdTe:V, Cl), as well as for the undoped specimen L825. The curves shown in Fig. 8, as well as those that are presented from here on, were normalized versus the photon flux, which was approximately constant (between 5×10^{12} and 3×10^{13} $cm^{-2}\,s^{-1}$).

The first noteworthy point is the sharpness of the peak corresponding to intrinsic PC. This is due to the steepness of the fundamental absorption edge of CdTe owing to the direct band-gap character of the optical transition. The strong decrease on the high-energy side of the spectrum indicates strong surface recombination.

The second point to note is the fact that the undoped crystal shows only the sharp peak at ~1.5 eV. Thus, independent of MCD, PC measurements tell us that the bands between 0.7 and 1.4 eV, observed for doped crystals, are really correlated with the presence of vanadium. Quite naturally, these bands bear a close resemblance to those found in the absorption spectra.[3,6,18]

A final point, of great interest, is that sample B19, which contains essentially V^{2+}, shows only a weak PC at room temperature in a spectral region (at ~0.8 eV), where B28 (V^{3+}) gives a large signal. The PC band at lower energies in Fig. 8 must therefore be labeled P_3 to maintain consistency with our MCD assignment to V^{3+} (Fig. 3). The largest contribution to the PC of B19 is found to occur above 1.0 eV and to extend to as high as 1.4 eV, in good agreement with our assignment[8] of the spectral features in this region to the photoionization of V^{2+}. Finally, the shift of band P_3 from 0.82 eV in Fig. 8 to 0.87 eV in Fig. 3 is thought to be related to the blue shift observed in absorption upon cooling. A small difference in calibration may also exist among the monochromators used in the different laboratories.

C. Spectral Response of Steady-State Photoconductivity at Variable Temperature

Detailed steady-state PC measurements were carried out for a series of temperatures on the semi-insulating sample B23. For clarity only three spectra are shown in Fig. 9. The modification of the intrinsic spectrum results from the temperature dependence of the band gap and of the PC gain G. We found a linear shift of its maximum of approximately 0.46 meV/K, in good agreement with that of the literature.[19] A similar figure was found in the

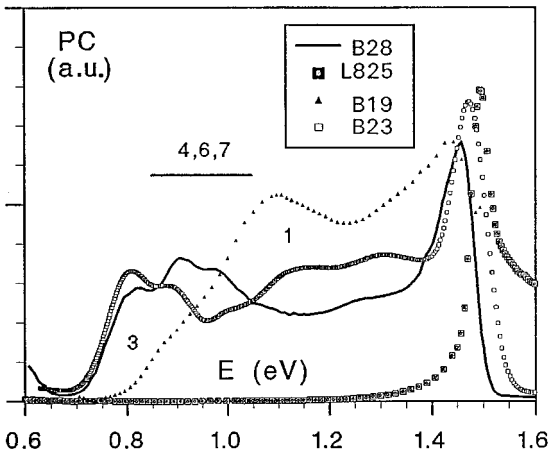

Fig. 8. Steady-state PC spectra at room temperature of Cl-codoped (B19), As-codoped (B28), and semi-insulating (B23) CdTe:V crystals. The spectrum of an undoped sample (L825) is also shown for comparison. Because the various spectra were taken between 290 and 320 K, one can observe a slight shift of the maximum of intrinsic PC.

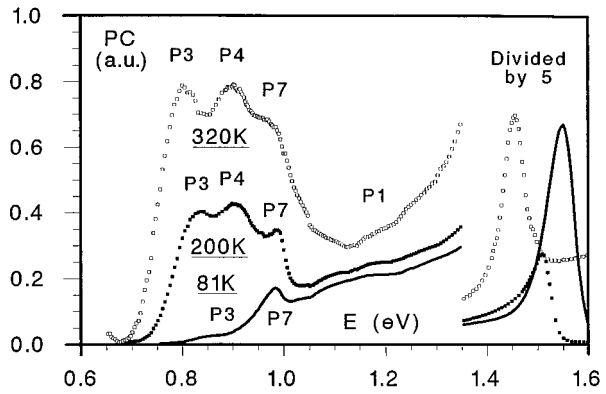

Fig. 9. Temperature dependence of the normalized steady-state PC for sample B23. Note that PC for $E \geq 1.35$ eV was divided by 5 so as to magnify the low-energy and highly structured sections.

course of similar measurements on other samples. Comparison of spectrum labeled 320 K with that of B23 of Fig. 8, obtained at 294 K, shows that the shift in energy of the maximum, of approximately 10 meV, indeed corresponds to that predicted by the law just mentioned. For energies higher than the band gap we can observe that the surface recombination is less important at 320 K than at room temperature. Here also, the magnitude of the maximum follows the temperature dependence of G, shown in Fig. 7. G is minimum at 200 K and is about 2 times higher at room and liquid-nitrogen temperatures, in agreement with our previous findings.

As for the temperature dependence of the extrinsic part in the most interesting low-energy region, the labeling of the resolved features follows that used for MCD (Fig. 3) and absorption (Figs. 5 and 6). The decrease of their magnitude between 320 and 200 K follows roughly that of the gain. Below 200 K, however, the change is drastic, and band P_3 has almost vanished at 81 K. Its width does not appear to vary significantly, and its height was found to follow $\exp(-W/k_BT)$, with $W \approx 30$ meV. Band P_3 also suffers a clearly observable linear energy shift of 0.23 meV/K, i.e., exactly half that of the band gap. In contrast with the above results, the positions of bands P_7 and P_4 (Fig. 9) are temperature independent. At 81 K, band P_4 occurs as a weak shoulder between P_3 and P_7.

5. PHOTOREFRACTIVE MEASUREMENTS

A. Experimental Arrangement

Photorefractive performances of sample B23 are analyzed in a two-beam-coupling experiment. The measurement of the strength of the photorefractive energy transfer gain from a pump beam toward a probe beam (from which we deduce the photorefractive gain Γ) as a function of the grating spacing provides two important parameters of the photorefractive effect: the electron–hole competition coefficient ξ_0, and the inverse of the Debye screening length k_0 (i.e., the effective trap density N_{eff}).[20] The expression of the gain with the grating spacing Λ (or grating wave number $k = 2\pi/\Lambda$), when one considers that the electron–hole competition factor is independent of the grating spacing, as is usually assumed in semiconductors, is[21,22]

$$\Gamma = \frac{2\pi {n_0}^3 r_{\text{eff}}}{\lambda \cos\theta} \frac{k_B T}{e} \frac{\xi_0 k}{1 + (k^2/{k_0}^2)}, \tag{4}$$

with ${k_0}^2 = [e^2/(\varepsilon k_B T)]N_{\text{eff}}$. θ is the half-angle between the beams inside the crystal; n_0, the linear refractive index of the material; r_{eff}, the effective electro-optic coefficient that depends on the crystal and the beam polarization orientations;[23] and ε, the dielectric constant. All these parameters are known from the literature.

The two experimentally determined parameters (ξ_0 and N_{eff}) depend on the deep-level characteristics through the well-known expressions[22]

$$N_{\text{eff}} = \frac{[V^{2+}][V^{3+}]}{[V^{2+}] + [V^{3+}]}, \quad \xi_0 = \frac{S_n[V^{2+}] - S_p[V^{3+}]}{S_n[V^{2+}] + S_p[V^{3+}]},$$

to which we add the linear absorption of the crystals $\alpha = S_n[V^{2+}] + S_p[V^{3+}]$. We consider here the optical generation of electrons and holes from V^{2+} and V^{3+}, respectively, with photoionization cross sections S_n and S_p.

The measurements are performed at the three wavelengths of 1.06 μm (1.17 eV), 1.32 μm (0.94 eV), and 1.55 μm (0.8 eV), given by two diode-pumped Nd:YAG lasers and a laser diode, respectively. The photorefractive gain is verified to be saturated with respect to the illumination for each wavelength. The absence of absorption gratings is checked by use of the symmetry properties of photorefractive gain. We measure the energy-transfer direction and then the sign of ξ_0 for the different wavelengths. By a direct measure of both the sign of the Pockels effect and the photorefractive gain relative to a fixed reference direction,[24] we determine that electrons are the majority carriers ($\xi_0 > 0$) at 1.06 μm, as was already measured on two other CdTe samples in previous studies.[25,26]

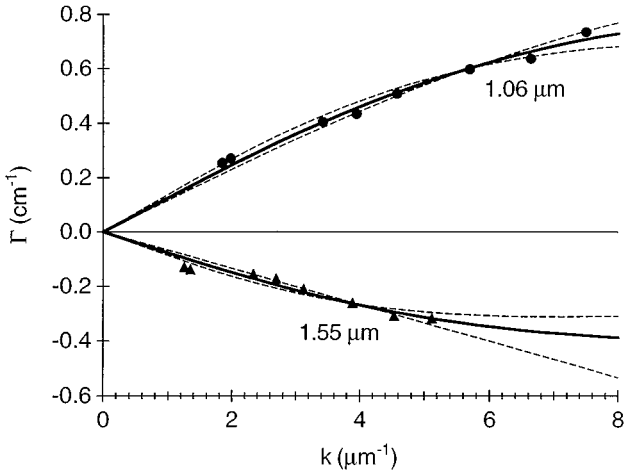

Fig. 10. Experimental photorefractive gain as a function of the grating spacing at wavelengths $\lambda = 1.06$ μm (●) and 1.55 μm (▲) for CdTe sample B23. The solid curves denote the best theoretical adjustments. The dashed curves represent the adjustment with $\sigma = 2\sigma_{\min}$. The photorefractive gain at 1.32 μm is nearly zero.

The CdTe:V sample (B23) is cut with a [111] face, (111) direction along the beam propagation direction. Other faces were $[1\bar{1}0]$, i.e., $(1\bar{1}0)$ direction along the beam polarization and $[11\bar{2}]$, i.e., $(11\bar{2})$ direction along the grating wave vector. With this geometry, the effective electro-optic coefficient is $r_{\text{eff}} = \sqrt{2/3}r_{41}$.

B. Experimental Results

Variation of the measured photorefractive gain Γ_m with the grating spacing is shown in Fig. 10. A high photorefractive gain (with opposite sign) is measured at 1.06 and 1.55 μm, whereas it is nearly zero at 1.32 μm. The adjustment of the experimental points by the theoretical curve gives us the two parameters ξ_0 and N_{eff} (except for $\lambda = 1.32$ μm, where we have only $\xi_0 \approx 0$). These adjustments are conducted with the same value of $r_{41} = 5.5$ pm V^{-1} (Refs. 18 and 27) for the three wavelengths and a refractive index of n_0 ($\lambda = 1.06$ μm) = 2.82 and n_0 ($\lambda = 1.55$ μm) = 2.74.[27] To obtain an estimate of the accuracy, we define the quadratic error between the experimental points $\Gamma_m(k_i)$ (at grating wave number k_i) and the theoretical value $\Gamma(k_i)$ as

$$\sigma^2(k_0, \xi_0) = \sum_i [\Gamma_m(k_i) - \Gamma(k_i)]^2. \tag{5}$$

We calculate the $\xi_0 = f(k_0)$ that minimize σ for a fixed k_0. We also calculate the minimum σ parameter, obtained for $\overline{\xi_0}$ and $\overline{k_0}$ and denoted $\sigma_{\min}$. We consider that k_0 is within the uncertainty domain when $\sigma[k_0, f(k_0)]$ is less than $2\sigma_{\min}$. We find that

At 1.06 μm, $\overline{k_0}^2 = 166$ μm^{-2} and $\overline{\xi_0} = 0.84$, with $100 < {k_0}^2 < 300$ μm^{-2} (which gives an uncertainty of 100%), and $0.78 < \xi_0 < 0.93$ (which gives an uncertainty of 18%);

At 1.55 μm, $\overline{k_0}^2 = 109$ μm^{-2} and $\overline{\xi_0} = -0.82$, with 50 $\mu m^{-2} < {k_0}^2$ (no upper limit of the value of ${k_0}^2$ can be determined), and $-0.94 < \xi_0 < -0.71$ (which gives an uncertainty of 28%).

We can see that if the electron–hole competition is strong at 1.32 μm ($\xi_0 \approx 0$), giving full compensation, it is rather low at 1.06 μm, where dominant carriers are electrons, and at 1.55 μm, where dominant carriers are holes. We note that the photorefraction measurements are consistent with the photoabsorption ones.

6. GENERAL DISCUSSION

A. Spectroscopic Assignments

We recall that the spectral distribution of the photocurrent $I_{\text{ph}}(h\nu)$ in the extrinsic region is given by the sum of the overall possible transitions (including crystal-field transitions $d \rightarrow d^*$ with subsequent thermally stimulated $d^* \rightarrow$ CB transitions, where CB denotes conduction band) involving a certain number of impurity levels:

$$i_{\text{ph}}(h\nu) = qAE\Phi_0 \sum_i N_i[\, f_i S_{ni}(h\nu)\mu_n\tau_n + (1 - f_i)S_{\text{pi}}(h\nu)\mu_p\tau_p], \tag{6}$$

where N_i are the concentrations of the levels, f_i is the occupation rate of the ith level, $S_{ni}(h\nu)$ and $S_{pi}(h\nu)$ are the photoionization cross sections of transitions from the ith level to the conduction band and from the valence band to level i. Here also A is a constant, depending on the geometry of the sample, and E is the applied electric field. Equation (4) derives from the fact that the optical emission rate is ${e_o}^n(h\nu) = {S_o}^n(h\nu)\Phi_o(h\nu)$ and from the basic equation $dn/dt = {e_o}^n N_i f_i$.[14]

The detailed assignment of the absorption spectrum of CdTe:V is still controversial. For example, the strongest absorption features above 1 eV were alternatively assigned without very convincing justification to V^{2+} (Refs. 3 and 11) or to V^{3+} (Ref. 6), whereas the weakest ones below 1 eV were assigned exclusively to V^{2+} (Ref. 3) or to both V^{2+} and V^{3+} (Ref. 11). As we show here, the measured spectrum obviously depends on the relative amounts of V^{2+} and V^{3+} in the investigated specimen. We found band P_2 in the same position in the low-temperature MCD (1.4 K, Fig. 3) and in the absorption (80 K, Fig. 5) spectra of sample B19 (basically V^{2+}). Furthermore, the band is absent in the room-temperature PC spectrum in the same sample (Fig. 8). We therefore confirm our earlier assignment[8] of P_2 to a transition having a dominant internal character [$^4A_2(^4F)$ excited state]. By contrast, band P_7 (Fig. 6), which is correlated with V^{2+} in view of the photoabsorption but which also shows up as a relatively sharp feature in the PC spectrum at liquid-nitrogen temperature (Fig. 9), is assigned to a transition to an excited state [$^4T_1(^4P)$], which is resonant with the conduction band.[3,28] These attributions for the spin-allowed bands of V^{2+} appear to be a clear confirmation of the previous ones.[10]

Band P_1, which occurs at ~1.15 eV in the MCD and absorption spectra of B19 and B23, is absent (or at best too weak to be detected) in those of B28. The same situation appears to hold in the case of PC (Fig. 8), and we therefore confirm our initial[8] assignment of the band to the photoionization of V^{2+} with an optical threshold at ~ 0.95 eV. Admittedly, however, one very puzzling and yet unexplained point is the absence of a clear photochromism for this band when crystal B23 is illuminated at either 1.55 or 1.06 μm. We also note that our interpretation for P_1 differs from those given in Refs. 5 and 29, whose authors prefer the alternative assignment to the photoneutralization of V^{3+} in view of the luminescence excitation spectrum of their crystals. At least part of those authors' arguments, however, is based on the fact that the stable existence of V^{2+} was doubtful at the time, a fact that is now contradicted by MCD in the case of our semi-insulating or n-type samples.

Our low-energy MCD results for B28 (bands P_3, P_4, and P_6) bear a very close resemblance to those found for V^{3+}, when it was substituted for Ga in GaAs (Ref. 30), and were assigned to the $^3A_2 \rightarrow {}^3T_1$ internal transition. The same assignment was also proposed in Refs. 5 and 29 in view of the $^3T_2 \rightarrow {}^3A_2$ luminescence band (threshold at ~0.54 eV) and its excitation spectrum. As compared with GaAs, the crystal-field parameter Dq is smaller in the case of CdTe because the $^3T_1$ state appears to be below ^1E (located by MCD). Although consistent with Tanabe–Sugano diagrams,[31] the assignment of the three MCD features to a purely internal transition is not completely satisfying. In the case of pure d orbitals for

the d^2 configuration, theory predicts[32] a negative MCD for the spin-forbidden line (as observed) and an S-shaped MCD (due to spin-orbit coupling) for the spin-allowed transition. This is indeed the situation that results for the isoelectronic d^2 ions Mn^{5+} (Ref. 32) and Ti^{2+} (Ref. 6) in tetrahedral symmetry. At this stage, we stress that the considered internal transition corresponds to a transfer of an electron from the vanadiumlike e orbital to the t_2 orbital, which strongly hybridizes with the host. The ligand–field picture is therefore not fully appropriate. An explanation of the different behavior of V^{3+} and Ti^{2+} requires theoretical research.

The blue shift (half that of the band gap) of P_3 under cooling implies its assignment to the VB $\rightarrow d^2$ charge-transfer process where VB denotes valence band. The complex temperature dependence of PC, however, is not yet understood.

In summary, the occurrence of two complementary processes in the P_3–P_6 region are proposed: (i) photoneutralization of V^{3+} leading to hole conductivity and (ii) crystal-field transition ($^3A_2 \rightarrow {}^3T_1$) of V^{3+}, with subsequent thermally stimulated $^3T_1 \leftrightarrow$ CB transfers (electron conductivity).

B. Photoionization Cross Sections

The insertion of vanadium in CdTe creates a deep level that corresponds to the two charge states V^{2+}/V^{3+}. These two charge states are responsible for the absorption and, as shown in the PC measurements, for the photogeneration of charge carriers at room temperature. The latter condition is a necessary one if the defect is to be the source of the photorefractive effect. The concentration in the two vanadium species is given by the EPR experiment and by the MCD measurements described in Sections 2 and 3. The EPR experiment gives us $[V^{3+}] \approx 6 \times 10^{15}$ cm^{-3}, whereas the MCD allows us to determine $[V^{2+}] \approx 5 \times 10^{15}$ cm^{-3} (Table 2).

The use of these two values gives, for the effective trap density, $N_{\text{eff}} \approx 2.7 \times 10^{15}$ cm^{-3}, from which we deduce $k_0{}^2 \approx 200\ \mu$m^{-2}, which corresponds to the experimental values.

Now, from ξ_0 and considering that the value of the absorption α (Fig. 5), corrected from a constant background absorption, is due only to a process that creates electrons and holes from a single defect under two charge states (V^{2+}/V^{3+} here), we deduce the two products $\alpha_n = S_n[V^{2+}]$ and $\alpha_p = S_p[V^{3+}]$ for each wavelength [using $\alpha_n = (\alpha/2)(1 + \xi_0)$ and $\alpha_p = (\alpha/2)(1 - \xi_0)$]. These values, together with the concentrations given in Table 2 above, allow us to calculate the photoionization cross sections. The ratio of electron and hole absorptions (α_n/α_p), and thus the ratio of the photoionization cross section, is given by the electron–hole competition coefficient only, whereas the absolute value of cross sections is determined by the value of the absorption α of the crystal.

We then deduce the following:

At 1.06 μm: ($\alpha = 1.6$ cm^{-1}), $S_n \approx 2.9 \times 10^{-16}$ cm^2, $S_p \approx 2.2 \times 10^{-17}$ cm^2;

At 1.32 μm: ($\alpha = 0.85$ cm^{-1}), $S_n \approx 8.6 \times 10^{-17}$ cm^2, $S_p \approx 7.2 \times 10^{-17}$ cm^2;

At 1.55 μm: ($\alpha = 0.58$ cm^{-1}), $S_n \approx 1.1 \times 10^{-17}$ cm^2, $S_p \approx 8.8 \times 10^{-17}$ cm^2.

The trends of these results correspond to the ones previously published.[33] We have a monotonic decrease of S_n with increasing wavelength, whereas S_p shows a maximum in the 1.3–1.5-μm region of the spectra, as already observed. The orders of magnitude for these cross sections are also kept, compared with the ones given in Ref. 33. The assumption that we use in our interpretation of the experimental results, that all of the absorption contributes to charge generation, is perhaps not totally warranted because of inadequate correction of the background or because of the presence of internal transitions. For example, our experimental data were processed assuming a constant background of absorption (considering the crystal absorption to be zero at $\lambda = 2\ \mu$m) for ease of use. Nevertheless, even if this assumption is not totally warranted, the results remain qualitatively the same; only the exact values of cross sections vary, and the features and the ratio of the photoionization cross sections remain the same.

7. CONCLUSION

In summary, we have performed a large number of spectroscopic experiments as well as photorefractive measurements in CdTe:V crystals with the goal of identifying the defect responsible for the photorefractive effect. We have extended earlier MCD studies and have further illustrated the use of the technique to monitor $[V^{2+}]$ and $[V^{3+}]$ simultaneously. Photoabsorption results are reported, for the first time to our knowledge. They confirm MCD and photo-MCD assignments. Furthermore, they indicate the existence of new features at ~0.95 eV (band P_6, V^{3+} related) and 1 eV (band P_7, V^{2+} related).

The spectral response of the steady-state PC of CdTe:V has been determined for n-type (Cl-doped), p-type (As-doped), and semi-insulating (sample B23) V-doped crystals and has been compared with that of an undoped one. These results confirm that vanadium is indeed the dominant carrier donor. They are consistent with MCD, which shows no noticeable feature for the undoped sample. Most of the bands found in MCD and absorption (except P_2) were found to be responsible for the generation of free carriers, a necessary condition for them to have an influence on the photorefractive effect. The thermal dependence of PC has also been measured for sample B23. The position of the various bands at 81 K correlates well with MCD (1.4 K) and absorption (80 K) results. Although their temperature dependence (shift, intensity) is not fully understood, it indicates that internal ($d \rightarrow d^*$) transitions are presumably followed by a subsequent thermally stimulated $d^* \rightarrow$ CB transfer.

The semi-insulating CdTe sample B23 has also been the object of a detailed photorefractive investigation. It demonstrates the predominance of hole carriers at 1.55 μm and electron carriers at 1.06 μm, in excellent agreement with the photoabsorption results. Electron–hole competition is very strong at 1.32 μm, leading to a complete cancellation of ξ_0 (corresponding to equal generation

of electrons and holes, $\alpha_n = \alpha_p$). The measured effective trap density was found to be in accord with the $[V^{2+}]$ and the $[V^{3+}]$ concentrations determined by MCD and EPR. Using the measured room-temperature absorption coefficient at each wavelength and the $[V^{2+}]$ and the $[V^{3+}]$ concentrations determined by MCD and EPR, we have also estimated the associated photoionization cross sections at the three studied wavelengths and have found them to be consistent with those published previously. Moreover, the self-consistency of our results gives very strong support to the correctness of our concentration determinations.

In sum, although it is well established that CdTe crystals may contain a large variety of defects,[34] it appears that most of our present physical results can be understood under the assumption that the photoconversion processes in V-doped crystals predominantly concern the V^{2+}/V^{3+} state. A few experimental facts remain unexplained. This condition applies, in particular, to the absence of a clear change of the absorption above 1 eV for our semi-insulating crystal when it was submitted to an illumination at 1.55 or 1.06 μm. This suggests competing processes and requires additional research. It follows from earlier theoretical considerations[35,36] and recent[37] experimental studies on ZnTe:V that the existence of the acceptor level V^{2+}/V^{+} relatively close ($\approx$0.4 eV) to the conduction band cannot be completely ruled out.

ACKNOWLEDGMENTS

Support for this research by Direction des Recherches Études et Techniques (grant number 94-063) is gratefully acknowledged. We are also indebted to one of the referees for his very stimulating criticism of our manuscript.

REFERENCES

1. Ph. Delaye, L. A. de Montmorillon, H. J. von Bardeleben, and G. Roosen, "Photorefractive wave mixing in undoped liquid encapsulated Czochralski GaAs at 1.5 μm: validation of photorefractive modeling," Appl. Phys. Lett. **64**, 2640 (1994).
2. H. J. von Bardeleben, J. C. Launay, and V. Mazoyer, "Defects in photorefractive CdTe:V: an electron paramagnetic resonance study," Appl. Phys. Lett. **63**, 1140 (1993).
3. R. Schwartz, M. Ziari, and S. Trivedi, "Electron paramagnetic resonance and an optical investigation of photorefractive vanadium-doped CdTe," Phys. Rev. B **49**, 5274 (1994).
4. H. J. von Bardeleben, V. Mazoyer, X. Launay, and J. C. Launay, "A comparative electron paramagnetic resonance study of vanadium in n-type, semi-insulating and p-type CdTe," Semicond. Sci. Technol. **10**, 163 (1995).
5. H. J. Schultz and J. Kreissl, "Optical and EPR properties of V and Ti ions in CdTe," Opt. Mater. **4**, 202 (1995).
6. P. Christmann, H. C. Alt, D. M. Hofmann, B. K. Meyer, J. Kreissl, R. Schwarz, and K. W. Benz, "Optically detected magnetic resonance investigations on titanium and vanadium ions in CdTe," Opt. Mater. **4**, 210 (1995).
7. B. Lambert, M. Gauneau, G. Grandpierre, M. Schoisswohl, H. J. von Bardeleben, J. C. Launay, V. Mazoyer, A. Aoudia, E. Rzepka, Y. Marfaing, and R. Triboulet, "Effective trap concentration in photorefractive CdTe:V and ZnCdTe:V crystals," Opt. Mater. **4**, 265 (1995).
8. B. Briat, F. Ramaz, A. Hamri, H. J. von Bardeleben, J. C. Launay, and V. Mazoyer, "Monitoring of V^{2+} and V^{3+} in vanadium-doped CdTe: a combined magnetic circular dichroism and electron paramagnetic resonance approach," Semicond. Sci. Technol. **10**, 1629 (1995).
9. H. J. von Bardeleben, C. Miesner, J. Monge, B. Briat, J. C. Launay, and X. Launay, "An electron paramagnetic resonance and magneto-optical study of vanadium in $Zn_xCd_{1-x}Te$:V," Semicond. Sci. Technol. **10**, 1 (1995).
10. P. A. Slodowy and J. M. Baranowski, "Absorption spectra of Ti(d^2), V(d^3), and Cr(d^4) ions in CdTe," Phys. Status Solidi B **49**, 499 (1972).
11. A. Aoudia, E. Rzepka, A. Lusson, A. Thomson-Carli, D. Schneider, Y. Marfaing, and R. Triboulet, "Crystal growth and characterization of CdTe doped with transition metal elements," Opt. Mater. **4**, 241 (1995).
12. E. Rzepka, Y. Marfaing, M. Cuniot, and R. Triboulet, "Deep centres for optical processing in CdTe," Mater. Sci. Eng. B **16**, 262 (1993).
13. L. A. de Montmorillon, Ph. Delaye, J. C. Launay, and G. Roosen, "Comparative study of CdTe and GaAs photorefractive performances from 1 μm to 1.55 μm," Opt. Mater. **4**, 233 (1995).
14. J. P. Zielinger and M. Tapiero, "Assessment of deep levels in photorefractive materials by transient photoelectric methods," J. Phys. (Paris) III **3**, 1327 (1993).
15. R. H. Bube, *Electronic Properties of Crystalline Solids* (Academic, New York, 1974).
16. J. Jouglar, C. Hetroit, P. L. Vuillermoz, and R. Triboulet, "Influence of growth parameters on CdTe low temperature thermal conductivity," J. Appl. Phys. **51**, 3171 (1980).
17. M. S. Kushwaha and S. S. Kushwaha, "Lattice dynamics of ZnTe, CdTe, GaP, and InP," Can. J. Phys. **58**, 351 (1980).
18. A. Partovi, J. Millerd, E. M. Garmire, M. Ziari, W. H. Steier, S. B. Trivedi, and M. B. Klein, "Photorefractivity at 1.5 μm in CdTe:V," Appl. Phys. Lett. **57**, 846 (1990).
19. A. Muranevich, M. Roitberg, and E. Finkman, "Growth of CdTe single crystals," J. Cryst. Growth **64**, 285 (1983).
20. M. B. Klein and G. C. Valley, "Beam coupling in $BaTiO_3$ at 442 nm," J. Appl. Phys. **57**, 4901 (1985).
21. N. V. Kukhtarev, V. B. Markov, S. G. Odulov, M. S. Soskin, and V. L. Vinetskii, "Holographic storage in electrooptic crystals. I. Steady state," Ferroelectrics **22**, 949 (1979); "Holographic storage in electrooptic crystals. II. Beam coupling–light amplification," **22**, 961 (1979).
22. F. P. Strohkendl, J. M. C. Jonathan, and R. W. Hellwarth, "Hole–electron competition in photorefractive gratings," Opt. Lett. **11**, 312 (1986).
23. J. C. Fabre, J. M. C. Jonathan, and G. Roosen, "$\bar{4}3m$ photorefractive materials in energy transfer experiments," Opt. Commun. **65**, 257 (1988).
24. G. Pauliat, M. Allain, J. C. Launay, and G. Roosen, "Optical evidence of a photorefractive effect due to holes in $Bi_{12}GeO_{20}$ crystals," Opt. Commun. **61**, 321 (1987).
25. Ph. Delaye, F. Bignon, G. Roosen, M. Tapiero, J. P. Zielinger, Z. Guellil, J. C. Launay, and V. Mazoyer, "Spectroscopic and photorefractive investigation of vanadium-doped cadmium telluride," Nonlinear Opt. **5**, 103 (1993).
26. J. C. Launay, V. Mazoyer, M. Tapiero, J. P. Zielinger, Z. Guellil, Ph. Delaye, and G. Roosen, "Growth, spectroscopic and photorefractive investigation of vanadium-doped cadmium telluride," Appl. Phys. A **55**, 33 (1993).
27. D. T. F. Marple, "Refractive index of ZnSe, ZnTe and CdTe," J. Appl. Phys. **35**, 539 (1964).
28. E. Rzepka, A. Aoudia, M. Cuniot, A. Lusson, Y. Marfaing, R. Triboulet, G. Brémond, G. Marrakchi, K. Cherkaoui, M. C. Busch, J. M. Koebel, M. Hage-Ali, P. Siffert, J. Y. Moisan, P. Gravey, N. Wolffer, and O. Moine, "Optical and thermal spectroscopy of vanadium-doped CdTe and related photorefractive effect," J. Cryst. Growth **138**, 244 (1994).
29. P. Peka, M. U. Lehr, H. J. Schulz, R. Schwarz, and K. W. Benz, "Energy levels of vanadium ions in CdTe," Appl. Phys. A **58**, 447 (1994).
30. A. Görger, B. K. Meyer, J. M. Spaeth, and A. M. Hennel, "Identification of spin, charge states and optical transitions of vanadium impurities in GaAs," Semicond. Sci. Technol. **3**, 832 (1988).

31. S. Sugano, Y. Tanabe, and H. Kamimura, *Multiplets of Transition Metal Ions in Crystals* (Academic, New York, 1970).
32. F. Ramaz, A. Hamri, B. Briat, V. Topa, and G. Mitroaica, "Magnetic circular dichroism and absorption study of photochromism in Mn-doped $Bi_{12}GeO_{20}$," Radiat. Eff. Defects Solids **136**, 1009 (1995).
33. G. Bremond, A. Zerrai, G. Marrakchi, A. Aoudia, Y. Marfaing, R. Triboulet, M. C. Bush, J. M. Koebbel, M. Hage-Ali, P. Siffert, and J. Y. Moisan, "Characterization and identification of the deep levels in V doped CdTe and their relationship with the photorefractive properties," Opt. Mater. **4**, 246 (1995).
34. W. Stadler, D. M. Hofmann, H. C. Alt, T. Muschik, B. K. Meyer, E. Weigel, G. Müller-Vogt, M. Salk, E. Rupp, and K. W. Benz, "Optical investigations of defects in $Cd_{1-x}Zn_xTe$," Phys. Rev. B **51**, 10619 (1995).
35. V. I. Sokolov, "Universal trends of changes in the positions of (0/+) and (0/−) levels of 3d impurities in II–VI compounds," Sov. Phys. Solid State **29**, 1061 (1987).
36. C. Delerue, "Théorie des ions de transition dans les semiconducteurs," Thesis (Université des Sciences et Techniques de Lille, France, 1989), p. 123.
37. P. Peka, M. U. Lehr, H. J. Schulz, U. W. Pohl, J. Kreissl, and K. Irmscher, "Vanadium centers in ZnTe crystals. I. Optical properties," Phys. Rev. B **53**, 1907 (1996).